AN INITIAL LOOK AT THE SUPERSONIC AERODYNAMICS OF TWIN-FUSELAGE AIRCRAFT CONCEPTS

Richard M. Wood, Samuel M. Dollyhigh, and David S. Miller
National Aeronautics and Space Administration
Langley Research Center
Hampton, Virginia

ICAS-82-1.8.3

Abstract

Results of two studies into the supersonic aerodynamics of twin-fuselage aircraft configurations are summarized. In the first study, a set of experimental data was obtained on a simple rectangular-wing twin-fuselage wind-tunnel model; this data was then used to evaluate prediction methods, assess favorable interference effects, and identify any unexpected or unpredictable aerodynamic phenomena. Results are presented which show that significant reductions in wave drag are possible through optimum body positioning and that existing aerodynamic prediction methods are adequate for making preliminary aerodynamic estimates. Several configuration concepts were theoretically explored in the second study, and results are presented which indicate the sensitivity of the twin-fuselage concept to various methods of integrating the aircraft components.

Nomenclature

b	wing span
C_D	drag coefficient
C_{D_F}	friction drag coefficient
C_{D_I}	lift-induced drag coefficient
C_{D_W}	wave-drag coefficient
C_L	lift coefficient
C_m	pitching-moment coefficient
C_n	yawing-moment coefficient
C_p	pressure coefficient
C_Y	side-force coefficient
D/q	drag per unit of dynamic pressure, m^2
ℓ	body or fuselage length
L/D	lift-drag ratio
M	Mach number
U_∞	free-stream speed
x	Cartesian coordinate in streamwise direction
y	Cartesian coordinate in spanwise direction
ΔC_D	incremental change in drag coefficient
Δx	incremental change in x coordinate
Δy	incremental change in y coordinate
α	angle of attack, deg
θ	body polar angle, deg (see fig. 1.)

Subscripts:

BODY	pertaining to the body
max	maximum value
min	minimum value
WING	pertaining to the wing

Introduction

Recent system studies (refs. 1 and 2) have indicated that significant performance improvements can be achieved for subsonic passenger and cargo aircraft by utilizing the novel concept of two fuselages. One study (ref. 1) showed that passenger seat miles per gallon could be increased by as much as 40 percent without the application of advanced engines, advanced materials, or aerodynamic benefits, but by simply employing two fuselages rather than the conventional single fuselage. In general, the benefits afforded by twin fuselages are an effective increase in wing aspect ratio, reduced wing weight due to a reduced wing bending moment, and reduced total fuselage weight when both single and twin-fuselage geometries are configured for the same number of passengers or payload. These benefits are independent of aircraft operating speed and should be equally applicable to supersonic as well as subsonic aircraft. The studies also alluded to but did not quantify possible adverse aerodynamic interference effects; however, aerodynamicists rely heavily on positive interference when configuring efficient supersonic aircraft and the concept of twin-fuselages offers a challenging opportunity to explore an additional multitude of component arrangements to maximize the performance of supersonic aircraft.

Theoretical results obtained from assembling a twin-fuselage aircraft by joining two AST-205 (ref. 3) configurations indicated that a doubling of fuselage volume could be obtained with little or no aerodynamic performance penalty. These results are reported in this paper and provided the motivation for further study into the adequacy of aerodynamic prediction methods and into other means of assembling twin-fuselage aircraft.

In order to assess the multitude of fuselage arrangements, sizes, and shapings, it is necessary for the prediction methods to treat general geometric components which may or may not be symmetrically arranged. The zero-lift wave drag may be computed by the far-field method of reference 4 and with the near-field surface panel method of reference 5; the latter method may also be used in computing the longitudinal and directional characteristics at lifting conditions. A wind-tunnel test program was conducted in which forces and moments were measured for a series of parametric variations of two bodies of revolution mounted on a rectangular wing. The two previously mentioned prediction methods were then evaluated by comparing computed and measured aerodynamic data.

Concurrently with the wind-tunnel testing, a theoretical study was conducted to examine several means of configuring the inboard region between the fuselages. Four practical but different approaches were examined and the results were summarized for this paper.

Discussion

The concept of employing two fuselages to improve supersonic aircraft performance opens a new technological arena in the areas of aerodynamics, stability and control, and structures. As with any idea, the development process begins by establishing methods for theoretically and experimentally assessing the merits of the concept and by exploring applications for the concept. Two aerodynamic prediction methods were evaluated and several configurations were aerodynamically explored to begin the development process for twin-body supersonic aircraft.

Evaluation of Prediction Methods

Discussion of Methods. The large number of possible twin-fuselage configurations to be explored makes the task of selecting a prediction method difficult, but extremely important. The major difficulty occurs because most aerodynamic analysis codes were written assuming geometric symmetry between the left and right sides; however, twin fuselages can be different sizes, different shapes, or longitudinally skewed which violates the symmetry assumption. Because of this arbitrary geometry requirement, only two aerodynamic codes were found to have adequate geometry representations; these were the PAN AIR code and a modified version of the far-field wave-drag (FFWD) code. The modified wave-drag code, which is limited to zero-lift wave-drag computations, employs the same area-rule solution technique as that of reference 4; however, the geometry definition was changed from a component-dependent (wings, fuselage, nacelle, vertical tail, etc.) scheme to a completely arbitrary, component-independent scheme.

The PAN AIR code and the FFWD code have both advantages and disadvantages in performing parametric geometry studies. The far-field method contains no strict requirements on matching component boundaries (i.e., wing to fuselage intersections). As a result of the code's relaxed geometry definition, it is well suited for analyzing parametric variations in the location of the two fuselages, however, the method provides a limited amount of interference information and no information on surface pressures. On the other hand, the near-field analysis method employed by the PAN AIR code provides this latter type or interference information in addition to the total drag values, but assembling the many geometries according to the strict rules governing the intersecting and matching of component boundaries becomes a tedious and time-consuming task. Both codes were applied to the physical geometry in the spirit of preliminary design and analysis; no attempt was made to represent separated flows or to adjust the linear-theory means of propagating disturbances along Mach lines.

Interfering Bodies. Previous experimental work in the area of supersonic interference concentrated on a wide variety of problems ranging from complete configuration optimization (refs. 6 and 7) to the simple interference between isolated components such as wings or bodies (refs. 8 and 9). These studies were a great benefit to the twin-fuselage investigation in that they provided a much-needed data base for performing preliminary evaluations of the theoretical methods. Presented in figure 1 are results from one such preliminary study in which theoretical and experimental data are presented for a reflection plane simulation of two interfering bodies (ref. 10). In the left portion of the figure, PAN AIR predicted and experimentally measured pressures are shown along two streamwise strips on a body of revolution in the vicinity of a reflection plane. For the side of body facing the reflection plane ($\theta = 0°$) and the side of body opposite the reflection plane ($\theta = 180°$), pressure data are presented for separation distances of $y/\ell = 0.10$ and 0.21. At both separation distances, excellent agreement was obtained between the theory and experiment. Especially notice that for the separation distance of $y/\ell = 0.10$ the nose shock at $x/\ell = 0.33$ and the reflective shock at $x/\ell = 0.50$ are both accurately predicted by the PAN AIR code; also, the different character of the pressure distributions for $\theta = 0°$ and $\theta = 180°$ is accurately predicted. The incremental variation in zero-lift drag due to varying the body position is presented in the right portion of figure 1. This shows that an optimum (minimum drag) body position does exist and results in a net zero-lift drag reduction of 100 counts. Both the PAN AIR and the FFWD codes predict drag trends and drag levels which are in acceptable agreement with the experimental data.

Interfering Bodies and Rectangular Wing. Despite the abundance of experimental data on interference effects, there is a void in the experimental data base for multiple-fuselage configurations. In an effort to fill this void, a generic, twin-fuselage wind-tunnel test program was conducted. Since the main purpose of the test program was to generate an initial set of twin-fuselage data and to evaluate theoretical methods, the main model design criteria were simplicity and versatility. The model consisted of two identical axisymmetric bodies of revolution with an effective fineness ratio of 10 (total length ℓ = 101.60 cm., maximum radius r = 5.08 cm.), and a rectangular planform wing having an aspect ratio of 1.8, a span of 50.80 cm., and a 3 percent circular arc airfoil. Figure 2 graphically depicts the wind-tunnel model test matrix where Δy denotes the distance between body centerlines and Δx denotes the longitudinal distance between the aft end points of the bodies. A photograph of the model in test section 1 of the Unitary Plan Wind Tunnel (ref. 11) is presented in figure 3. The experimental test conditions were a Mach number of 2.70 and a Reynolds number of 6.56×10^6 per meter; the model angle of attack was varied from -4 to 12 degrees.

Theoretical results were obtained on the generic twin-body wind-tunnel model using both the FFWD code and the PAN AIR code. As shown in figure 4, the PAN AIR input geometry consisted of 18 networks representing the model and 8 wake

networks; all impermeable surfaces were represented by mass-flux-type boundary conditions except for the balance housing where the panels are near Mach inclined and according to reference 5, velocity-type boundary conditions produce better solutions.

Theoretical and experimental zero-lift wave-drag values for various longitudinal ($\Delta x/b$) and lateral ($\Delta y/b$) separations of the bodies are presented in figure 5. For both $\Delta x/b$ values of 0.0 and 0.5, varying Δy shows that an 18 percent reduction in wave drag can be obtained by separating the bodies to a $\Delta y/b$ value of 0.85. However, due to the nature of the generic twin-fuselage model, which has a skin-friction drag (C_{DF}) value of 0.00844, the total zero-lift drag reduction is only 6 percent. Comparing theory with experiment for the two cases of varying Δy reveals that both theoretical methods do an adequate job of predicting the trends, but the FFWD code does a better job of predicting the drag levels. The change in zero-lift wave drag due to variations in the longitudinal separation distance ($\Delta x/b$) at a constant spanwise separation ($\Delta y/b = 0.25$) is also shown in figure 5. For this situation, experimental results show that the minimum zero-lift wave drag occurs at zero longitudinal separation. Both theories underpredicted the wave drag for the maximum longitudinal separation distance.

From the results shown in figure 6, a correlation can be made between minimum drag and maximum lift-to-drag ratio at various spanwise separation distances for longitudinal separation distances of $\Delta x/b = 0.0$ and 0.5. For the $\Delta x/b = 0.0$ case, the optimum separation for drag minimization is a $\Delta y/b$ of 0.85, whereas, a separation distance of 0.35 results in the most aerodynamically efficient configuration. A similar type of relationship is evident for the $\Delta x/b = 0.5$ case; here the minimum drag occurs at two $\Delta y/b$ values of 0.55 and 0.75, but the maximum $(L/D)_{max}$ value occurs only at a $\Delta y/b$ of 0.55. Also notice that there are no additional increases in maximum lift-to-drag ratio as a result of body skewing. These observed results indicate that strong interactions exist between lifting and thickness effects for the twin-fuselage configuration and that configuration optimization should not be limited to the zero-lift condition.

Both theoretical and experimental longitudinal force and moment results for the unskewed ($\Delta x/b = 0.0$) configuration with a body lateral separation ($\Delta y/b$) of 0.25 are presented in figure 7. Theoretical results are shown for the PAN AIR code and the Middleton and Carlson method of reference 12 as implemented in the code of references 13 and 14. Results from the latter method were obtained for two representations of the configuration's lifting surface; in one representation only the rectangular wing was included in the lifting surface definition and in the other representation the fuselage and wing were included. In general, the PAN AIR code did a much better job of predicting the longitudinal aerodynamics; the most dramatic indication of this is displayed in the variation of pitching-moment coefficient with lift coefficient. Because both prediction methods give similar results for the wing alone and the inclusion of a fuselage representation in either method produces an improvement in predicted pitching moment, it is concluded that both the fuselage lift and the fuselage-induced lift on the wing must be included and that these effects are better accounted for in the PAN AIR code.

The directional aerodynamic characteristics provided not only some very interesting results, but also a most difficult challenge for the prediction methods. In fact, only the PAN AIR code could treat asymmetrical geometries at lifting conditions. Typical side-force and yawing-moment coefficients are presented in figure 8 as a function of angle of attack. The results on the left side of the figure show that the effect of skewing the fuselages from an $\Delta x/b$ value of 0.0 to 0.5 produces a negative yawing moment and positive side force whose magnitude increases with angle of attack; the results in the right side of the figure show these effects to be enhanced with increased spanwise separation distance. A review of existing experimental directional data for an SST-type configuration (ref. 15) reveals that the experimentally measured yawing moment values for the large angles of attack relate to 3 to 4 degrees angle of sideslip. The PAN AIR code overpredicts the directional aerodynamic coefficients for the asymmetric twin-fuselage configurations and indicates that the yawing moments is a net result of asymmetric body axial forces (couple effect) and a side force due to the asymmetric interference effects. These large differences between theory and experiment could be due to the observed flow separation on the aft portion of the bodies which resulted from strong interference effects. Flow separation on the aft portion of the bodies would create a forward shift in the side force center of pressure resulting in the experimentally observed reduction in yawing moment.

Concluding Remarks on Prediction Methods

Even though the PAN AIR code underpredicted the zero-lift drag and overpredicted the directional problems associated with the asymmetric configurations, the code did an excellent job of matching the trends and incremental effects associated with varying the fuselage position both symmetrically and asymmetrically. As stated previously, the code is the only available theoretical method available which handles arbitrary geometries at all conditions. The modified version of the far-field wave-drag code did an excellent job of predicting the zero-lift wave-drag levels and trends for the various body positions. As a result, future supersonic aerodynamic analysis of multi-fuselage configurations can reliably use the modified far-field wave-drag code for the zero-lift wave-drag calculations and the PAN AIR code for the analysis of lifting and directional aerodynamic characteristics.

Configuration Studies

Concurrent with the investigation to obtain experimental data on a parametric variation of twin-body configuration geometries and to evaluate the applicability of existing theoretical methods, some initial aerodynamic system studies were being conducted to evaluate the component integration aspect of the twin-fuselage concept.

These studies focused their attention on establishing the guidelines for component integration. Theoretical methodology employed was limited to the far-field wave-drag theory and the Middleton and Carlson lifting-surface theory. Configurations which were studied represented complete aircraft geometries and consisted of two fuselages, wings, pods, and horizontal and vertical tails.

Successful aerodynamic utilization of the beneficial interference between fuselages depends on whether twin bodies can be integrated with other airplane components and result in increased aircraft performance; i.e., (L/D). However, for an aircraft configuration, the aerodynamic integration involves trades between drag-due-to-lift, as well as wave drag and skin friction. Practical considerations, such as the relationship of the passenger seating arrangement to fuselage cross-sectional area, tend to favor two smaller fuselages over a single large fuselage for large capacity transport configurations. Still, for the twin-body arrangement, a substantial increase in skin friction must be offset by decreases in wave drag and drag-due-to-lift.

Twin-Fuselage Derivative of AST-205 Configuration

The first of the configuration studies utilized the AST-205 (Advanced Supersonic Technology) configuration geometry (ref. 3) to examine the effect of fuselage separation on both drag and $(L/D)_{max}$ at a supersonic cruise speed of Mach 2.70. The baseline vehicle (separation distance equal to zero) is an AST-205 with the fuselage volume doubled by doubling the cross-sectional area (and holding the length constant). As shown in the inset sketches of figure 9, the twin-body configurations were generated by joining two AST-205's with an appropriate part of the original wing. Fuselage separation distance is nondimensionalized by the original AST-205 wing span and separations were examined out to a $\Delta y/b$ value of 1.0, which would represent two AST-205's with wing tips touching. The wing area and total configuration span were allowed to increase with increased fuselage separation distance and no attempt was made to resize any of the aircraft components. The trends in the individual drag components on the left of figure 9 are as anticipated. Induced drag, C_{D_I}, (at $C_L = 0.1$) decreases and skin friction increases with separation distance as wing-span and area increase. The characteristics of wave drag versus body separation are similar to the trends observed in the previously discussed wind-tunnel test, in that the variation in wave drag has two local minimums associated with it, one at a $\Delta y/b$ value of 0.2, and an absolute minimum at a $\Delta y/b$ value of 0.8. The trend in $(L/D)_{max}$ with fuselage separation is shown on the right. After an initial slight drop, the $(L/D)_{max}$ rapidly increases, then breaks over and reaches a peak at approximately the body separation at which maximum (zero-lift) favorable interference occurs. Since about half of the total $(L/D)_{max}$ increase is achieved at a separation of 0.3 (approximately 40 feet), further configuration study will be concentrated here because this body separation appears to be achievable in a practical configuration.

Further Arrow Wing Configurations

Figure 10 illustrates four of the configuration types that were studied. Type 1 had an arrow wing planform that was held constant as the fuselages were moved laterally; type 2 was an M-wing series in which the center-wing geometry varied with fuselage spacing in the same way as it varied in the twin-body derivative of the AST-205; type 3 had an outboard arrow wing and an unswept sharp leading edge center wing with a chord length equal to the arrow wing root chord; and type 4 had a center engine package connecting the fuselages. Type 4 body spacing was not varied, but was determined to be a $\Delta y/b$ value slightly less than 0.2 by the required engine package size. For each different lateral spacing, the wing was resized so that all of the configurations had the same estimated wing loading. All of these configurations were modeled with uncambered wings and uncambered body-of-revolution type fuselages. The wave drag was calculated using the far-field wave-drag method which was previously shown to be acceptable for assessing the trends.

In figure 11, estimates of configuration performance are presented for a limited, but practical range of fuselage separation distances; in this figure, the maximum lift-to-drag ratio serves as a measure of performance. This figure contains several unexpected results that required a more detailed look at the integration of twin bodies into a configuration. Of all the configurations, the type 1 configuration, which exhibited the least benefit on $(L/D)_{max}$ due to increased body spacing, was penalized by a change in wing volume with fuselage separation. For this configuration, an increase in wing volume with the increase in fuselage separation occurs; this results in an interaction between fuselage spacing and configuration volume that offsets a large portion of the favorable interference effects. The M-wing (type 2) and rectangular inner wing (type 3) configurations both reach the maximum $(L/D)_{max}$ at a fuselage separation of approximately 0.3. However, the wave drag of the rectangular inner wing configuration was consistently 10 percent higher and, as a result, the M-wing configuration was the most efficient. The performance results for the configuration on which the inner wing was replaced by a structurally integrated propulsion pod were expected to be higher than shown in the figure. The engine package was believed to be an ideal connector because it is structurally thick, aerodynamically thin, locates the engines on the vehicle centerline, and frees the wing for additional flap area. Because the propulsion-pod planform and the wing planform were both counted in the configuration planform area, the elimination of the associated wing volume was expected to reduce the wave drag substantially. However, the wave drag was 30 percent higher than the M-wing configuration for the same lateral body spacing.

This 30 percent higher wave drag can be partially explained by the fuselages being at less than optimum spacing; a detailed look at the wave-drag area distributions revealed that this type of configuration has a much rougher distribution than the other three configurations. This lack of smoothness could be attributed to the wing geometry and led to the following examination of component effects which resulted in some general conclusions about the inner wing; reasons for the good performance of the M-wing configuration also become more evident.

Wave-drag calculated values for an isolated pair of AST-205 fuselages and an isolated pair of AST-205 outer wing panels are shown in figure 12 as a function of the lateral separation distance parameter, $\Delta y/b$. In a wave-drag sense, these two pairs of components are incompatible with lateral separation. In the right portion of the figure, the total wave drag of the wing panels decreases to a minimum value at $\Delta y/b = 0.3$ where the drag of the bodies is decreasing but still large, then the drag of the wing panels increases to the interference-free value at $\Delta y/b = 0.57$ (hash mark on dashed line) and no further drag changes occur with increased separation distance. On the other hand, the body drag decreases slowly with separation distance and reaches a minimum at $\Delta y/b$ value of about 0.7 which is after the wing-panel drag has already increased to the interference-free value. Further increases in separation only result in body drag increases until the body interference-free condition is reached (hash mark on solid line). This total drag analysis indicates that this pair of fuselages and this pair of wing panels (without the addition of volume to smooth the area distribution) in a wave-drag sense are not compatible at reasonable lateral separation distances.

This incompatibility is more dramatically emphasized in the right portion of the figure which shows only the wave drag for the $\theta = 0°$ Mach-sliced area distribution. As described in the wave-drag and area-rule discussion presented in reference 4, the total wave drag is obtained by averaging the individual drags obtained from Mach-sliced area distributions around the configuration from -90° below the configuration to +90° above the configuration. Accordingly, the $\theta = -90°$ and $\theta = +90°$ drags have absolutely no variation with lateral separation distance and the $\theta = 0°$ drag experiences the most dramatic variation with lateral separation distance. Because there is no center wing panel connecting the outer wing panels, as the outer wing panels are separated, the $\theta = 0°$ area distribution is also separating into two distinct area distributions having large wave drag. This drag reaches a maximum at a $\Delta y/b$ value of about 0.5 just before the body drag reaches a minimum at $\Delta y/b = 0.55$. This clearly demonstrates the wave-drag incompatibility of these two pairs of configuration components. The integrated propulsion-pod configuration and, to a lesser degree, the rectangular inner-wing configuration have increased wave drag compared to the M-wing configuration because they both have component and wave-drag properties similar to those just discussed. This occurs primarily because these two configurations have either no inner wing or because the inner wing has not been properly area ruled for wave-drag minimization.

The incorporation of swept, inner-wing panels between the fuselages is one practical means of preventing adverse wing interference from offsetting favorable interference on twin-fuselage configurations of the type studied.

Concluding Remarks on Configuration Studies

Conclusions that have been reached so far in the aerodynamic integration of twin fuselages into an AST configuration are that aerodynamic benefits occur at reasonable fuselage separation distances. Twin-body configurations require more careful aerodynamic integration than single-body configurations. The interrelationship between wing and fuselage volumes is particularly sensitive and requires careful component (inner wing, outer wing, and fuselage) integration to prevent adverse wing interference from offsetting favorable fuselage interference. These relationships can be expected to vary considerably with design Mach number, fuselage fineness ratio, and wing planform.

References

1. Houbolt, J. C.: Why Twin-Fuselage Aircraft? Journal of Astronautics and Aeronautics, April 1982, p. 26.
2. Maglieri, D. J.; and Dollyhigh, S. M.: We Have Just Begun to Create Efficient Transport Aircraft. Journal of Astronautics and Aeronautics, February 1982, p. 26.
3. Martin, G. L.; and Walkley, K. B.: Aerodynamic Design and Analysis of the AST-204, -205, and -206 Blended Wing-Fuselage Supersonic Transport Configuration Concepts. NASA CR-159223, March 1980.
4. Harris, R. V., Jr.: An Analysis and Correlation of Aircraft Wave Drag. NASA TM X-947, 1964.
5. Moran, J.; Tinoco, E. N.; and Forrester, T. J.: User's Manual Subsonic/Supersonic Advanced Panel Pilot Code. NASA CR-152047, February 1978. Jones, R. T.: Minimum Wave
6. Drag for Arbitrary Arrangement of Wings and Bodies. NACA TN-3530, February 1956.
7. Ferri, A.; Clarke, J. A.; and Ting, L.: Favorable Interference in Lifting Systems in Supersonic Flow. Journal of the Aeronautical Sciences, vol. 24, no. 11, pp. 791-804, November 1957.
8. Friedman, M. D.; and Cohen, D.: Arrangement of Fusiform Bodies to Reduce the Wave Drag at Supersonic Speeds, NACA TN-3345, Nov. 1954.
9. Ferri, A.; and Clarke, J. H.: On the Use of Interfering Flow Fields for the Reduction of Drag at Supersonic Speeds. Journal of Aeronautical Sciences, vol. 24, no. 1, pp. 1-18, January 1957.
10. Gapcynski, J. P.; and Carlson, H. W.: A Pressure-Distribution Investigation of the Aerodynamic Characteristics of a Body of Revolution in the Vicinity of a Reflection Plane at Mach Numbers of 1.41 and 2.01. NACA RML54J29, 1955.
11. Jackson, C. M., Jr.; Corlett, W. A.; and Monta, W. J.: Description and Calibration of the Langley Unitary Plan Wind Tunnel. NASA TP-1905, November 1981.

12. Middleton, W. D.; and Carlson, H. W.: Numerical Method of Estimating and Optimizing Supersonic Aerodynamic Characteristics of Arbitrary Planform Wings. Journal of Aircraft, vol. 2, no. 4, July-Aug. 1965, pp. 261-265.
13. Middleton, W. D.; and Lundry, J. L.: A System for Aerodynamic Design and Analysis of Supersonic Aircraft, Part 1 - General Description and Theoretical Development, NASA CR-3351, 1980.
14. Middleton, W. D.; Lundry, J. L.; and Coleman, R. G.: A System for Aerodynamic Design and Analysis of Supersonic Aircraft, Part 2 - User's Manual. NASA CR-3352, 1980.
15. Shrout, B. L.; and Fournier, R. H.: Aerodynamic Characteristics of a Supersonic Cruise Airplane Configuration at Mach Numbers of 2.30, 2.96, and 3.30. NASA TM-78792, Jan. 1979.

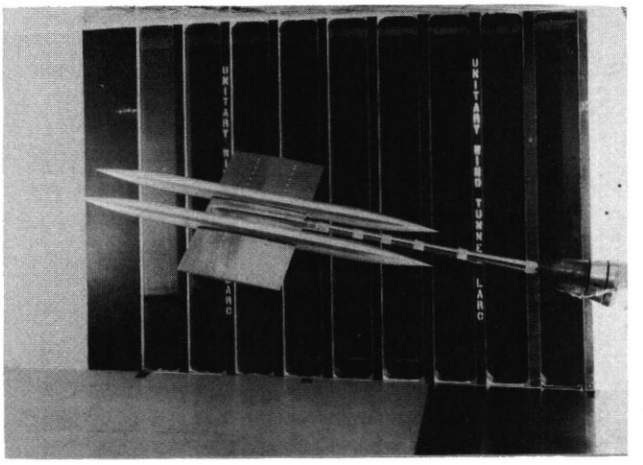

Figure 3. Photograph of twin-body model.

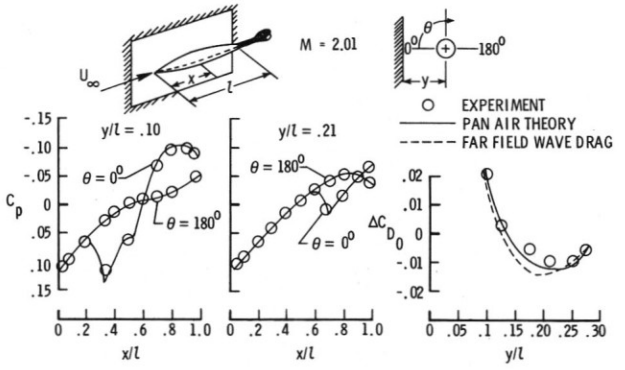

Figure 1. Twin-body interference effects simulated by a body of revolution in the vicinity of a reflection plane at M = 2.01.

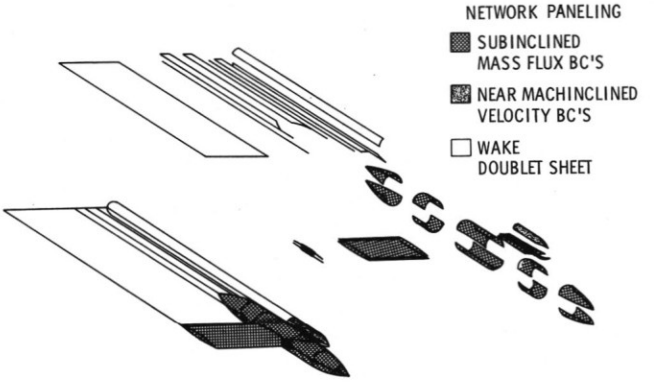

Figure 4. Illustration of typical PAN AIR input geometry and surface boundary conditions.

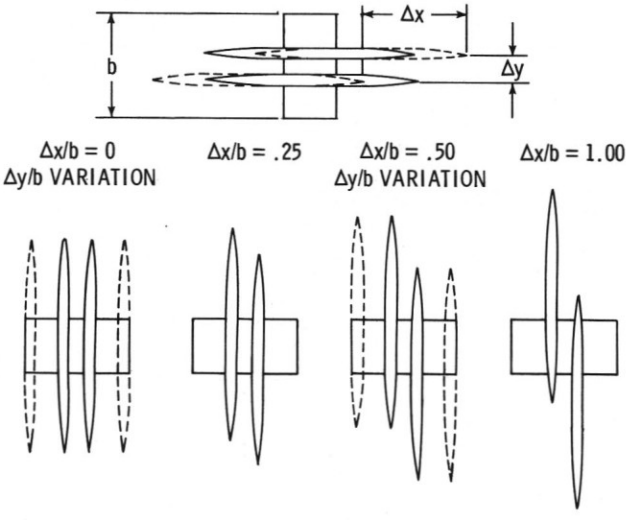

Figure 2. Parametric variation of wind-tunnel model body positions tested.

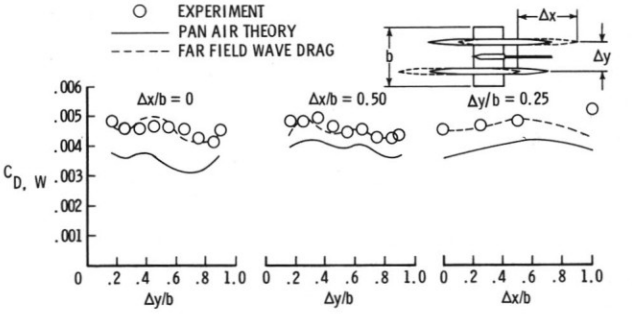

Figure 5. Experimental and theoretical variations in zero-lift wave drag with body position at M = 2.70.

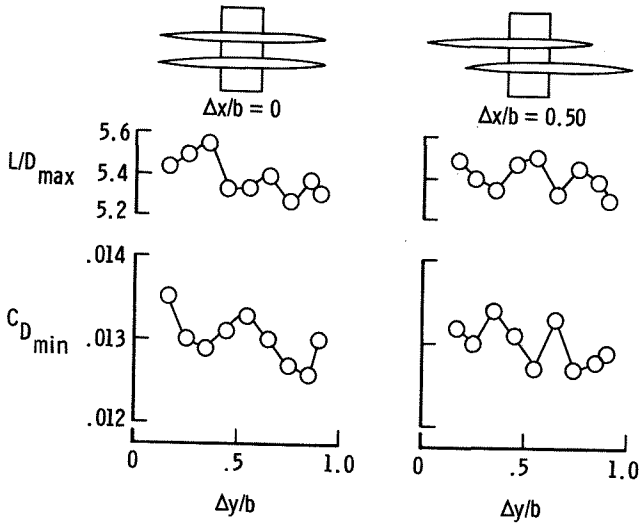

Figure 6. Effect of body lateral positioning on minimum drag at maximum lift-to-drag ratio at M = 2.70.

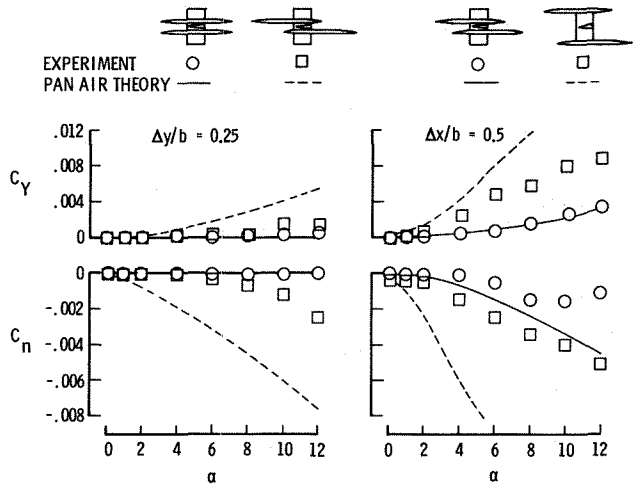

Figure 8. Typical theoretical and experimental directional characteristics of several twin-body configurations at M = 2.70.

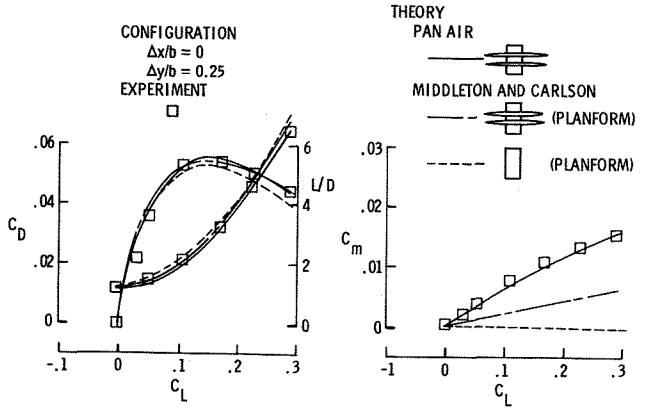

Figure 7. Typical theoretical and experimental longitudinal aerodynamic characteristics of the twin-body model at M = 2.70.

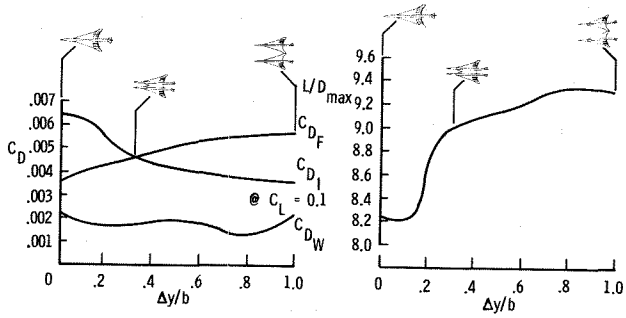

Figure 9. Effect of fuselage lateral positioning on drag and maximum lift-to-drag ratio at M = 2.70.

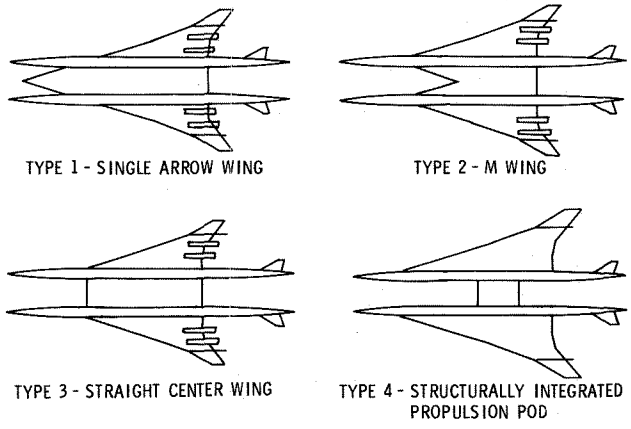

Figure 10. Illustration of the four inner-wing concepts.

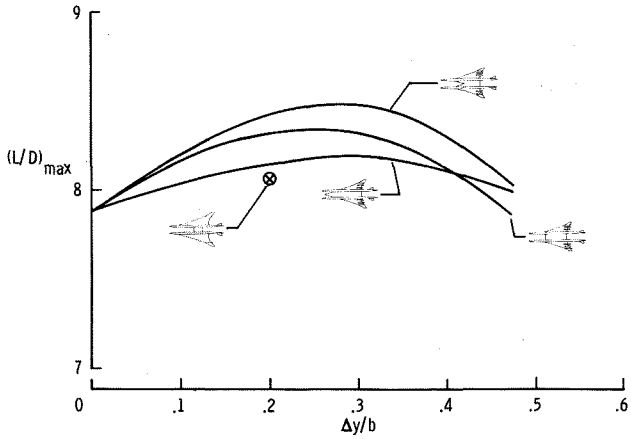

Figure 11. Variation in maximum lift-to-drag ratio due to fuselage lateral positioning for four different inner wing geometries at M = 2.70.

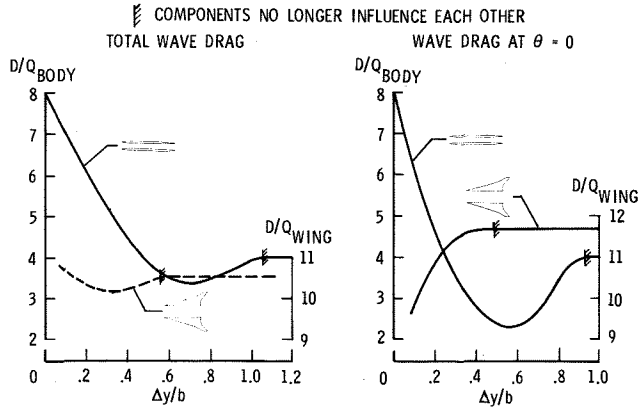

Figure 12. Variation in zero-lift wave drag with lateral separation of wings and bodies at M = 2.70